

Central European Journal of Chemistry

The photocatalytic degradation of 17α -ethynylestradiol by pure and carbon nanotubes modified TiO_2 under UVC illumination

Research Article

Radina Kralchevska¹, Maria Milanova¹, Mirjana Bistan², Albin Pintar², Dimitar Todorovsky^{1*}

¹University of Sofia, Faculty of Chemistry, 1164 Sofia, Bulgaria

²Laboratory for Environmental Sciences and Engineering, National Institute of Chemistry, SI-1001 Ljubljana, Slovenia

Received 7 November 2011; Accepted 23 January 2012

Abstract: Commercial product Degussa TiO2 P25, sol-gel produced TiO2 and TiO2 modified by carbon nanotubes addition (5% of the TiO2 mass) are tested as photocatalysts for the degradation of endocrine disrupting compound 17α-ethynylestradiol (1 μM aqueous solution). The molecular and crystal structure, phase composition, crystallite size, specific surface area, pore average diameter, their area and volume distribution, morphology, IR and UV/Vis spectra of the catalysts are characterized. HPLC is used for estrogen analysis. The sorption ability and photocatalytic activity (measured by degradation rate constant and percentage of the pollutant conversion) of the catalysts under UV (17 W, emission maximum at 254 nm) irradiation is determined. Full destruction of the pollutant is reached after 30 min irradiation in presence of Degussa P25. The performance of some of the catalysts is compared with literature data for their activity under 365 nm-illumination.

Keywords: Photocatalysis • TiO₂ • Estrogens • Sol-gel method • Carbon nanotubes © Versita Sp. z o.o.

1. Introduction

The steroids 17β -estradiol (E2) and 17α -ethynylestradiol (EE2, Fig. 1) [1], along with estrone (E1) and estriol (E3) are among the emerging pollutants of the aquatic environment. A major source of hormone steroids is livestock waste entering the environment via wastewater treatment plant effluents or untreated discharges. Normally the median concentration of EE2 in sewage effluents is rather low - between 1 and 3 ng L-1 [1,2]. However, in vitro studies have shown that exposure of wild fish to only 0.1 ng L⁻¹ of EE2 may provoke feminization in some species of male [1,3]. These concentrations are rather close to the present detection limits of most analytical techniques causing serious difficulties in its analysis [4]. One can assume that although EE2 was not always detected, it may still be present in some effluent samples. Concentrations of E2 up to 20 ng L-1 were reported in effluents from STW plants [5].

Most important processes that play a role in the removal of estrogens are: adsorption, aerobic or anaerobic degradation, anoxic biodegradation and photolytic degradation. Special attention is paid on advanced processes, including photolytic reactions which allow high removal of recalcitrant compounds.

Photocatalytic degradation of E2 on immobilized ${\rm TiO_2}$ was first reported by Coleman *et al.* [6]. In their later works [7,8], as well as in other papers [9,10], it was shown that photocatalysis coupled with photolysis is much more effective in degrading the estrogens than photolysis alone.

Degradation of E2 in water by Degussa P25- TiO_2 photocatalysis has been investigated by Ohko *et al.* [11]. It is shown experimentally and theoretically that the estrogenic activity of E2 is lost in the first step of the photocatalytic reactions.

Li Puma *et al.* investigated the degradation of multicomponent mixtures of E1, E2, EE2 and E3 by UVA and UVC photocatalysis in slurry with Degussa P25-TiO₂. Under UVA irradiation, the degradation of E3 was not significant; however, E1, E2 and EE2 were removed reaching respectively 49, 20 and 25% conversion after

^{*} E-mail: nhdt@wmail.chem.uni-sofia.bg

Figure 1. Molecular structure of EE2.

180 min of irradiation. Under UVC the conversions of E2, EE2 and E3 after 180 min were 60% [9].

Many types of UV sources offering various wavelength illumination (UVA [8,9,12], UVC [9,13]) and different power (150 W xenon lamp [6,10,13], 125 W Philips high-pressure mercury lamp [8], 15 W [12,13]), placed at variant distances from the treated solution have been applied. The reported efficiency of E2 degradation is 50% after 40 min to 98% after 3.5 h [6,10], 90% after 20 min [10], 97% after 4 h or 98% after 1 h of illumination depending on the type of illumination [13]. The first-order rate decomposition constant (min⁻¹) varies depending of treatment conditions: 0.033, 0.050 [10], 0.106 [8], 0.15 for E2 and 0.086 for EE2 [14].

Investigations of the effect of doping on the ${\rm TiO}_2$ photocatalytic efficiency are rather limited. It was found that the addition of 2 mol% Ag or Pt to ${\rm TiO}_2$ has no effect on the photocatalytic degradation or mineralization of all the endocrine disrupting compounds (EDCs) at concentrations found in water [12].

In our previous investigations, the photocatalytic activity of N-doped sol-gel prepared ${\rm TiO_2}$ and of microcomposites consisting of ${\rm TiO_2}$ and carbon nanotubes was studied for the first time under UVA ($\lambda_{\rm max}$ =365 nm) or halogen lamp irradiation.

The aim of the present paper is to investigate the photocatalytic degradation of EE2 under the action of shortwave UV illumination in presence of commercially available Degussa ${\rm TiO_2}$ P25 or sol-gel prepared ${\rm TiO_2}$ as well as of composite with 5% carbon nanotubes. The later material has not been used for treating of waste waters containing estrogens yet. The structure, phase composition, morphology and spectral properties of the prepared catalysts were studied and their sorption ability and photocatalytic activity were determined.

2. Experimental procedure

2.1. Materials

Commercially available Degussa TiO_2 P25 (Degussa-Hüls AG, mentioned in the text as P25), tetrabutyl-orthotitanate $Ti[OC_4H_o]_4$ (Fluka, purum, >97%), C_7H_7OH

(p.a., 99.8%), multi-walled carbon nanotubes MWNT-L-P (purity 80%, diameter 10-30 nm, delivered by Sunny Co. Ltd., China, preliminary purified/activated by 0.5 h boiling in conc. HNO_3 , labeled in the text as NT), methanol (for HPLC, purity 99.9%, Sigma-Aldrich) were used as starting materials in the present study. As model pollutant, estrogenic compound 17α -ethinyl estradiol (EE2, Sigma-Aldrich, 98%, HPLC grade) was applied.

2.2. Synthesis of catalysts

 ${\rm TiO_2}$ was prepared (Fig. 2) at ambient temperature by dissolving 0.026 mol ${\rm Ti(OC_4H_9)_4}$ in 40 mL of absolute ethanol. After 10 min, water-ethanol solution consisting of 12 mL H₂O (pH=3, HCl) and 65 mL of ethanol was added dropwise from a burette (a drop per 2 s). The obtained gel was aged for 24 h, ground in mortar and heated at 700°C (or 350°C) for 3 h in air.

The TiO₂-NT (Fig. 2) was obtained [15] adding (at vigorous stirring) the weighed amount of NT (5% of the mass of expected TiO₂) to the 0.026 mol Ti(OC₄H₉)₄ solution in 40 mL of absolute ethanol just after beginning of hydrolysis provoked by addition of mixed ethanolwater solution consisting of 12 mL water (pH=3) and 60 mL of absolute ethanol. After aging of the sol (24 h), the gel was ground, heated at 400°C for 3 h and cooled to room temperature in moderate N, flow to avoid the NT oxidation. The content of NTs was chosen following findings in [16] for the best results reached at similar concentrations of the modification agent. As expected, accounting for the conditions of the TiO2-NT composite preparation, there is no appreciable degradation of the NTs during the synthetic process. Determined (by hightemperature ignition of the samples) carbon content in the final product agrees (within the limits of ±0.4%) with the value, calculated from the ratio of components in the initial solution (similar results are reported in [17]).

2.3. Catalysts characterization

The content of nitrogen in the prepared sample was determined by means of the elemental analyzer Vario EL III V5.018.

X-ray diffractograms were taken by Siemens D-500 powder diffractometer (CuK_{α} , 40 kV, 30 mA) equipped with secondary monochromator to exclude K_{β} light. Quantitative analysis of diffractograms was performed by the Rietveld method using the program BRASS [18]. Thus, the lattice parameters, the average crystallite size and the phase composition ratio of the obtained materials were calculated.

The IR spectra (4000-400 cm⁻¹) were recorded on a Bruker model IFS 25 Fourier transform spectrometer (resolution < 2 cm⁻¹) at room temperature in KBr pellets. The film morphology of the same samples was observed

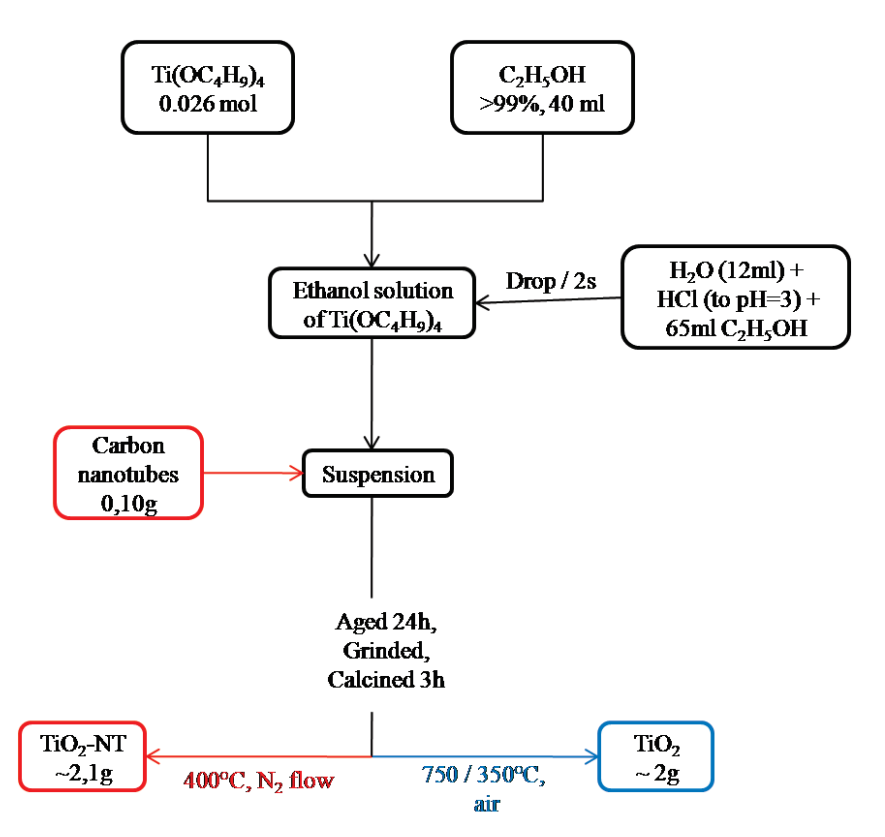


Figure 2. Scheme of the preparation of TiO, and TiO, carbon nanotubes composite.

by scanning (JEOL JSM 35CF) and transmission (HRTEM JEOL JEM 2100, 200 kV) electron microscopy. The surface area and porosity were measured by $\rm N_2$ adsorption-desorption by means of Micromeritics ASAP 2020 MP/C instrument. Before measurement, the samples (approx. 0.3 g) were degassed at 200°C. UV/Vis diffuse reflectance spectra of the powdered specimens were registered by means of a UV/Vis spectrophotometer (Perkin Elmer, model Lambda 40P) equipped with a Praying Mantis accessory.

2.4. Photocatalytic tests

Stock solution of EE2 (3 g L⁻¹) was prepared in methanol and stored in a freezer (-20°C) as recommended in [19]. Shortly before the experiments, working solution with concentration of 0.3 mg L⁻¹ (1.012 μ M) (containing 0.01% methanol; such an ethanol concentration is used in [8]) was prepared using ultrapure water (18.2 M Ω cm) and was added directly to the reactor for the photocatalytic tests. The working solution as well as aliquots withdrawn during the oxidation was stored for not more than 24 h in a refrigerator.

The photocatalytic activity of examined catalysts were tested in a batch slurry reactor (Fig. 3) at the following conditions: volume of reaction suspension $250~\text{cm}^3$, catalyst concentration 0.5~g L⁻¹,

magnetic stirring speed 600 rpm, and air flow rate (330 mL min-1). The reached agitation of the slurry excludes the influence of transport phenomena on the adsorption and photo degradation reactions kinetics. After a 30 min "dark" period (for the establishing of equilibrium of the sorption process), the system was illuminated by a 17 W UV lamp with λ_{max} =254 nm immersed perpendicularly in the suspension in a quarz hollow jacket. The double-walled constructed reactor ensures constant cooling of the investigated suspension by outer water flow (~5°C) using a thermostat (Julabo, model F25). The temperature of the suspension was always maintained between 19 and 21°C. The aliquots from solution exposed to irradiation for certain periods of time were filtered through a Whatman filter (0.45 µm pores) and subjected to subsequent analysis.

2.5. Analytical procedure

A solid phase extraction method for water sample analysis based on previous reports [19-21] was applied for sample pre-concentration. Calibration curve for EE2 is shown on Fig. 4. Each sample was analyzed twice by means of isocratic HPLC technique and average values were further considered. The uncertainty of HPLC analysis was characterized by the relative standard deviation of the signal (0.04%), calculated from three

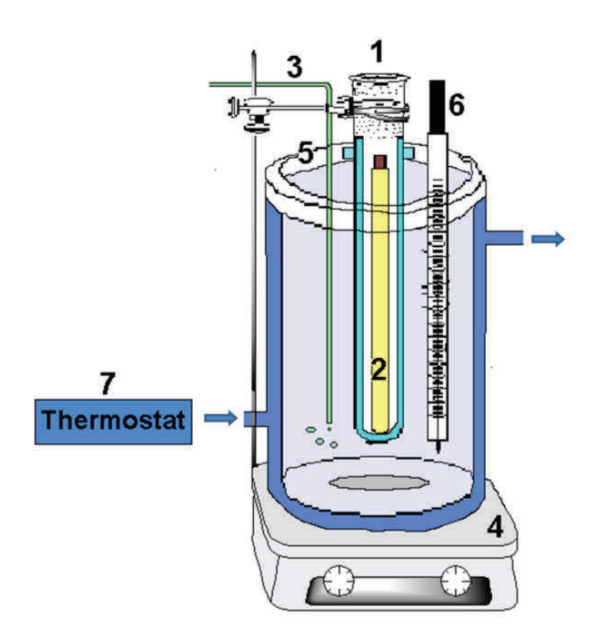


Figure 3. Experimental device for photocatalytic tests: 1 - Pyrex tap water cooling jacket (or quartz hollow jacket, when 17 W UV lamp with \$\lambda_{max}=254\$ nm is applied), 2 - lamp [halogen (VIS), UV (\$\lambda_{max}=365\$ nm or 254\$ nm)], 3 - constant air flow (330 mL min¹), 4 - magnetic stirrer (600 rpm), 5 - double-walled reactor (equipped with water-cooling jacket, connected to a thermostat), 6 - thermometer (temperature of the slurry is carefully observed and maintained between 19 and 21°C), 7 - thermostat (adjusted to maintain low temperatures of circulating water (~5°C), in order to compensate the heating power of the lamps and to assure constant temperature of the reaction suspension).

parallel analyses of a sample containing 0.3 mg L $^{-1}$ EE2. The data obtained were plotted in coordinates (C/C $_0$)/t and -ln(C/C $_0$)/t, where C $_0$ represents initial concentration after the dark period and C stands for concentration after t min irradiation. Apparent first order reaction rate constants of the overall degradation process were determined.

3. Results and discussion

3.1. Catalyst characterization 3.1.1. Crystal structure and phase composition

X-ray diffractogram of the sol-gel calcined (at 700°C) TiO_2 is shown in Fig. 5. The product interplanar distances (Table 1) are about 0.1-0.2% decreased (for rutile) or increased (for anatase) compared with the reference materials. Accordingly, the lattice parameters (Table 2) are changed in the respective directions. TiO_2 is a well-known material with a tendency to have anisotropic growth. This can explain the slight elongation of the c-axis for the product obtained at 700°C .

The crystallite size of the sol-gel catalyst significantly grows with the heating temperature (Table 2) but remains (after heating at 700°C) lower than that of the

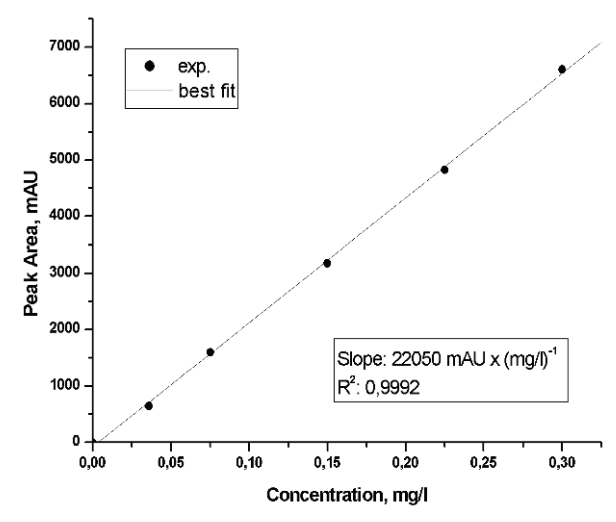


Figure 4. Calibration curve for HPLC determination of model pollutant EE2.

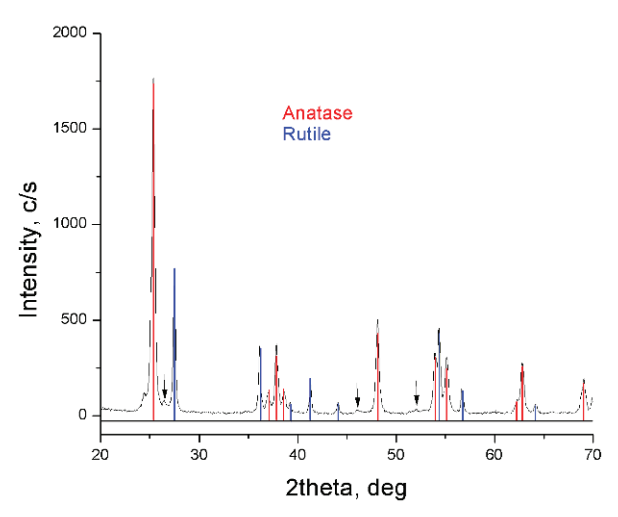


Figure 5. X-ray diffractograms of sol-gel synthesized TiO₂. Traces of an unidentified phase are shown with arrows.

commercial product. It is slightly increased compared to that of catalysts obtained at 500-550°C (20 – 22 nm) [22,23] and significantly smaller than crystallites of material obtained at 700°C by other authors, applying similar preparation methods (56 nm) [24].

The content of rutile in the high-temperature sol-gel product is higher than in the commercial product. The relatively high heating temperature of the ${\rm TiO_2}$ sol-gel (700°C) catalyst could be one of the reasons for this effect but the crystallite's size ratio does not agree with such a supposition. Probably other factors are also responsible for the increased rutile content.

3.1.2. Morphology

Fig. 6 shows SEM images of the studied catalysts. The sol-gel synthesized TiO₂ has a globular structure with grains considerably larger than those of the commercial

Table 1. Interplanar distances (d, n×10⁻¹⁰ m) and relative peak intensities (I, ‰) of the catalysts.

JCPDS 43-1295, TiO _{1.04}		JCPDS 77-0442, rutile		JCPDS 84-1286, anatase		hkl	TiO₂ (prepared at 700 °C)	
d	ı	d	ı	d	I		d	I
				3.5140	999	101	3.5204	360
		3.2557	999			100	3.2493	999
2.481	999					110	2.4881	559
		2.4944	434			101		
2.381	720					101	2.3801	100
				2.4283	62	103		
				2.3755	190	004		
				2.3305	72	112	2.3325	30
		2.3021	64			200	2.2982	80
		2.1932	169			111	2.1886	300
		2.0591	60			210	2.0558	110
				1.8911	249	200	1.8917	150
				1.6981	158	105	1.6880	789
				1.6652	155	211	1.6668	90

Table 2. Lattice parameters, size of crystallites and phase composition of the studied samples.

Sample	Parameters	Anatase	Rutile	
	a, b, Å	3.77600	4.59370	
JCPDS 78-2485 (rutile) JCPDS 73-1764 (anatase)	c, Å	9.48600	2.95870	
001 B0 70=1704 (unatase)	V, 10 ⁶ pm ³	135.25	62.43	
Degussa	Crystallite size, nm	45	56	
TiO ₂ P25	Content,%	82	18	
	a, b, Å	3.7808(4)	4.5898(5)	
	c, Å	9.506(1)	2.9562(4)	
TiO ₂ , produced at 700°C	V, 10 ⁶ pm ³	135.88	62.28	
	Crystallite size, nm	29	40	
	Content,%	70	30	
	a, b, Å	3.7827(7)		
	c, Å	9.472(2)		
TiO ₂ , produced at 350°C)	V, 10 ⁶ pm ³	135.53		
	Crystallite size, nm	9.4		
	Content,%	100		

product, 200-500 nm in size for the material obtained at 350° C and up to 1 μ m after heating at 700° C, inclined to agglomeration and sintering with formation of blocks a few micrometers in size.

Fig. 7 presents TEM image of the sol-gel prepared ${\rm TiO_2}$ with 5% NTs. ${\rm TiO_2}$ crystallites (approx. 10×10 nm and smaller) are seen situated along the tubes as well as assembled probably around nanotube active places (outlets, *etc.*). Vigorous stirring has to be applied in the course of synthesis in order to decrease the assembly.

3.1.3. Specific surface area and porosity

Fig. 8 shows nitrogen adsorption—desorption isotherms of the samples examined. The isotherm of the commercial product is rather similar to the one observed in [25] and (following [26]) can be described as type IV with type H3 hysteresis loops (appeared at p/p $_0$ = 0.85–1.0); the latter suggesting [27] materials with slit-like pores due to the particle aggregation or assembly. The sharp drop of N $_2$ adsorbed amount in desorption curve indicates mesoporosity of the products.

The sol-gel prepared (700°C) product shows the same type of isotherm with H2 type of hysteresis, with an inflection of nitrogen adsorbed volume at $p/p_0 = 0.45$ representative of well-developed mesoporosity [28]. The large hysteresis is attributed [29] to the existence of pore cavities larger than the openings. The TiO_2 annealed at 350°C has a quite different isotherm. The general profile of the TiO_2 -NT isotherm reveals the composite character of the sample, showing some similarities with the isotherm of sol-gel prepared (350°C) material. This is to be expected accounting for the similar temperature

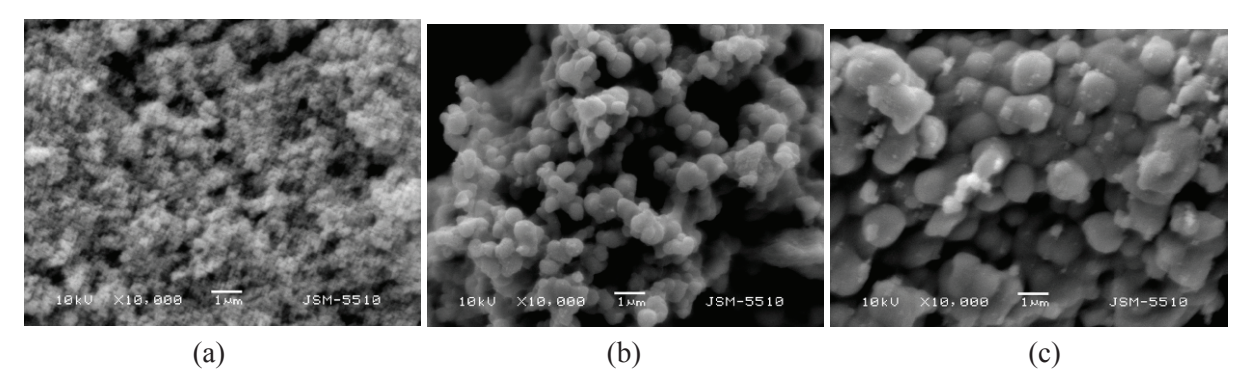


Figure 6. SEM images of Degussa TiO, P25 (a), sol-gel synthesized TiO, heated at 350°C (b) and 700°C (c).

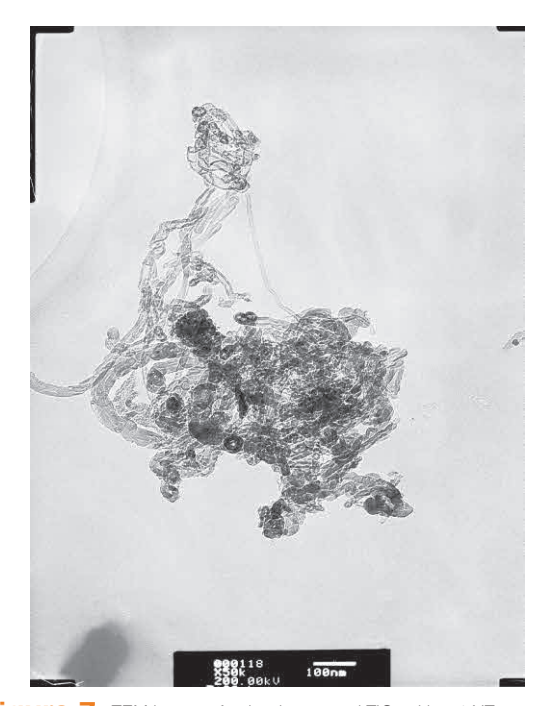


Figure 7. TEM image of sol-gel prepared TiO₂ with 5% NTs.

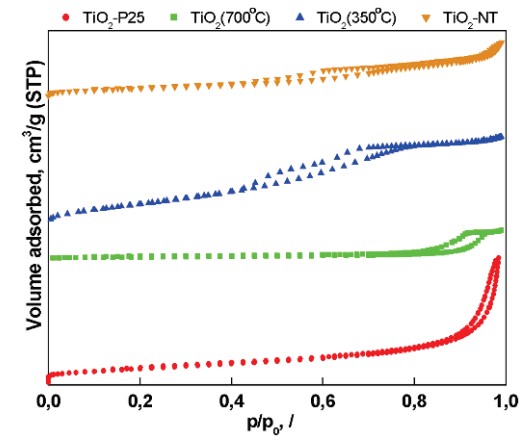


Figure 8. N₂ adsorption–desorption isotherms of Degussa TiO₂ P25, sol-gel produced (at 350 and 700°C) TiO₂ and TiO₂-NT.

of the ${\rm TiO_2}$ synthesis in both samples. The difference above p/p₀ \approx 0.45 has to be ascribed to the presence of NT.

Fig. 9 represents the specific volume and area occupied by the ensembles of pores (17 Å - 3000 Å) of the studied catalysts with respect to their average diameter, calculated by the Kruk-Jaroniec-Sayari method. As far as the pollutant molecule diameter is ~15 Å, pores above this width are namely of interest. Results for the specific area and the pore diameter, volume and area are summarized in Table 3. It is seen that the investigated materials exhibit porous structure, however the low-temperature annealed pure TiO, does not contain micropores (<4.6 Å). The average pore diameter and the total pore volume strongly depend on the calcination temperatures, the former increasing and the latter decreasing with the temperature increase. It seems that both parameters of the TiO₂-NT composite are driven by the dominating mass of TiO2. The pore distribution as a function of pore diameter (Figs. 9b-d) supports the above made conclusions.

It is well known that the surface area strongly depends on the material's heating temperature. Accordingly, the literature data on this parameter for pure ${\rm TiO}_2$ vary in a rather wide interval, even for products prepared by similar methods - from 59.2 m² g¹ for a product obtained at 400°C [30] to 0.08 m² g¹ obtained at 700°C [24]. The later, rather low surface area can be attributed to the formation of significantly larger crystallites (56.4 nm). Sample densification with the temperature increase is also observed in the present work (especially in the temperature interval 350-400°C, Table 3), but the surface area after heating at 700°C remains much higher than the one reported in [24].

The specific surface area of the TiO₂-NT composite is significantly lower than the one reported in [17] (114 m² g⁻¹) probably due to differences in NT parameters used in the cited and in the present work. The average pore size diameter is rather close to the 8.5 nm found

Table 3. Textural properties of the synthesized catalysts.

Parameter		Catalyst			
	Degussa	Sol-gel TiO ₂ ,		TiO ₂ -NT,	
	TiO ₂ P25	350°C	700°C	400°C	
BET surface area, m² g⁻¹	52.0	105.0	7.3	34.4	
Total pore volume, cm³ g⁻¹	0.17	0.13	0.04	0.08	
Average pore diameter (BHJ), Å	125.4	51.4	198.6	88.7	
Micropore (<4.6 Å) volume, ×10 ⁻⁵ , cm ³ g ⁻¹	3.1	*	0.6	9.8	
Micropore area, m ² g ⁻¹	1.89	*	0.11	1.29	

^{*} Not observed

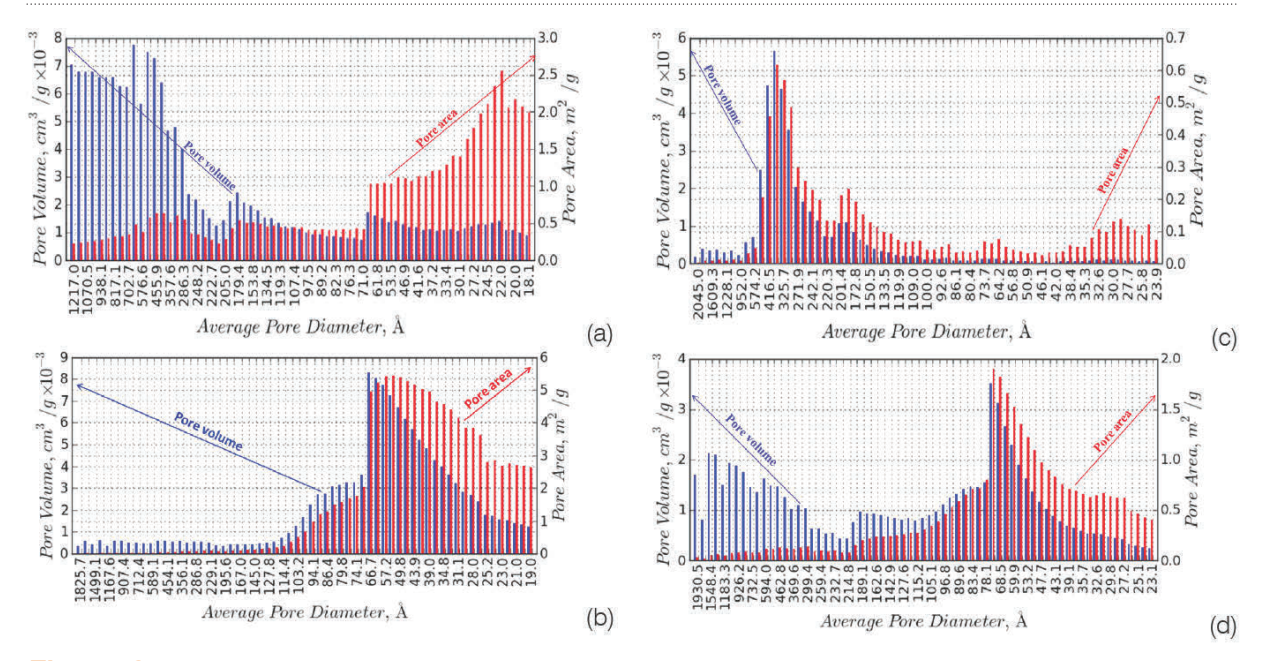


Figure 9. Pore volume and surface area distribution as a function of pore diameter for Degussa TiO₂ P25 (a), sol-gel produced TiO₂ heated at 350°C (b) and 700°C (c) and TiO₂-NT composite (d).

in [16] for the composites with almost the same NT content. The pore area shows monomodal distribution around pores with an average diameter of about 7 nm, rather similar to the low-temperature annealed pure TiO₂. The pores volume distribution resembles bimodal one (Fig. 9d), influenced by the small increase of the synthesis temperature (compare with Fig. 9c) and, probably, by the NT presence.

3.1.4. IR and UV/Vis spectra

The IR spectra of the studied catalysts are shown in Fig. 10. Data on band positions in the studied catalysts, according to literature data and the present results, are summarized in Table 4. The broad absorption band with a maximum around 3410 cm⁻¹ is characteristic for OH-stretching vibration of surface hydroxyl group and peak at 1630 cm⁻¹ is assigned to HO- bending of physically adsorbed water. The literature data for the vibration modes of anatase skeletal OTiO bonds vary widely (436-502 cm⁻¹, Table 4). In our samples they appeared

at 519-663 cm⁻¹ (a similar anatase band at 638 cm⁻¹ is reported in [31]) and result in 2-3 overlapping bands, in which the position and relative intensity most probably depend on the variations in the crystal structure/ crystallites size. The presence of NT causes slight red shifts of the most intensive band.

The UV/Vis diffuse reflectance spectra of synthesized materials are shown in Fig. 11. It can be seen that the commercial product Degussa TiO₂ P25 exhibits some absorption in the visible part of the spectrum. It is known that TiO₂ powders show absorption in the wavelength region longer than 400 nm due to the presence of Ti³⁺, which can be formed as a result of TiO₂ reduction at elevated temperatures [34,35]. Accounting for the Degussa TiO₂ P25 production mode [35,36], such reduction seems possible. The absorption of visible light by the low-temperature sol-gel obtained TiO₂ is due mainly to its beige color resulting in the presence of traces of carbon from the starting materials. It is known that complete burning of carbon traces in similar

Table 4. Bands (cm⁻¹) in the IR spectra of studied complexes.

Band								
origin	[32]	[28]	[30] [33]	[33]		This work* TiO₂, sol-gel, °C		TiO ₂ -NT
					Degussa P25			
						350	700	
OH- stretching	3410	3400, 2930 2850		3400	3408, 2917 2889	3439, 2959, 2855	3408, 2937, 2855	3440, 2930, 2880
HO- bending	1630			1630	1645	1657	1625	1655
Ti-O-Ti	502		495, 436	500	663, 559sh	655sh, 623, 521sh	621, 519	645sh, 621sh, 580
NH ₃		1380						
N in TiO ₂ (N-H)		1450, 1230 1090		1440				

(a) (b) 2,0-2,0 **Absorbance** Absorbance 1,5 1,0 1,0 0,0 1000 1500 2000 2500 3000 3500 4000 1000 1500 2000 2500 3000 3500 4000 Wavenumbers cm⁻¹ Wavenumbers, cm⁻¹ 2,0 (c) (d) 2,0 Absorbance Absorbance 1,5 1,0 1,0 0,0 0,0 1000 1500 2000 2500 3000 3500 4000 1000 1500 2000 2500 3000 3500 4000 Wavenumbers, cm⁻¹ Wavenumbers cm⁻¹

Figure 10. IR spectra of Degussa TiO, P25 (a), sol-gel prepared TiO, at 350°C (b) and 700°C (c) and TiO, -NT (d).

materials takes place above 500°C [37]. It is possible, however, that Ti³+, produced by a reduction process provoked by the remaining carbon, may have an impact on the visible light absorption. Such a hypothesis needs EPR spectroscopy verification. Despite the absorption, the preliminary experiments show that the low-temperature annealed product exhibits rather low photocatalytic activity and further study with this material was suspended.

The optical band edge of the sol-gel produced TiO_2 (700°C) exhibits a slight red-shift (up to 400 nm) with

respect to that of the commercial product. It can be due to the higher rutile relative content. Its content in Degussa P25 is 18-20%, and the band gap of pure anatase is usually noted at 3.23 eV and of pure rutile phase at 3.02 eV. The smaller red-shift in the low-temperature obtained product can be related to a decrease in crystallinity of the samples rather than to change of crystal structure [38].

The low reflectance of the ${\rm TiO_2} ext{-NT}$ composite is due to its black color.

Table 5. Sorption ability and apparent degradation rate constants obtained during the photolytic/photocatalytic oxidation of model pollutant over various catalysts.

Nº	Catalyst	Sorption,	λ _{max} = 254 r	nm, 17 W	λ _{max} = 365 nm, 150 W3		
		%	Rate constant, n×10 ⁻³ min ⁻¹	Correlation coefficient	Rate constant, n×10 ⁻³ min ⁻¹	Correlation coefficient	
1	Photolysis	-	38.7 ± 0.3	0.90.9316	26.8 ± 0.1	0.9671	
2	Sol-gel TiO ₂	18.2	53.8 ± 0.1	0.9918	102.6 ± 0.4	0.9461	
3	TiO ₂ -NT	80.7	$(80.2\pm0.5)^{1}$ $(3.73\pm0.0001)^{2}$	0.9847			
			Average: 58.1 ± 0.5	0.9126			
4	TiO ₂ P25	26.8	315.5 ± 0.0001		$(346.1 \pm 0.0001)^{1}$	0.9999	
	-				$(10.5 \pm 5.0)^2$	0.8974	
					Average: 77.8 ± 2.0	0.5715	

¹First stage of the process.

³Detailled results will be published elsewhere.

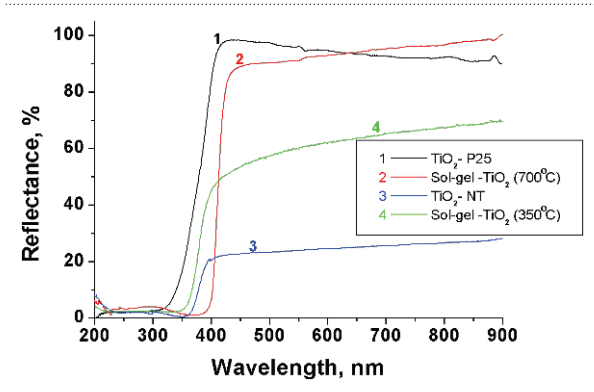


Figure 11. UV/VIS diffuse reflectance spectra of examined catalyst samples.

3.2. Sorption ability and photocatalytic activity 3.2.1. Sorption ability

Data listed in Table 5 show that the sorption ability depends strongly on the nature of the catalyst applied in the photocatalytic system. Specific surface area is an important but not a crucial factor determining the catalysts sorption performance. Despite its much smaller BET surface area (Table 3), the sol-gel produced (at 700°C) oxide shows with only ~30% lower sorption ability than the commercial product.

Addition of a small amount of NTs to the sol-gel prepared TiO₂ catalyst leads to more than a 3-fold increase of the sorption ability compared to P25 despite the significantly larger surface area of the latter (Table 3). Similar results were obtained for the E2 sorption. Our results are in harmony with those reported in [39]. Studying the adsorption of EE2 and BPA on carbon nanotubes, the authors [39] show that, in spite of the fact that the adsorption is controlled by the surface sorption sites, it is influenced by the molecular conformation of EDCs as well.

3.2.2. Photocatalytic degradation

Typical kinetics of the pollutant degradation resulting in the photolytic and heterogeneous photocatalytic process

is shown in Fig. 12 (assuming pseudo-first order of the reaction). The values of reaction rate constants of both processes are summarized in Table 5. The degree of estrogen degradation is presented on Fig. 13. Some data (that will be published in more details elsewhere) on the same estrogen destruction under UVC irradiation (λ_{max} =365 nm, high-pressure mercury 150 W lamp) are also included for comparison.

TiO₂ P25 shows much higher efficiency than the solgel product. The reasons for this effect are of special interest. Accounting for the much larger BET specific surface area of the commercial product (Table 3), one can assume it to be a main factor determining the photocatalytic activity. However, the above mentioned small difference in the sorption ability of the two types of catalysts show that this parameter hardly can play a major role in the activity of examined catalysts. Bubacz et al. [40] also pointed out that the photodegradation process is not BET surface area limited. Possibly, the difference can be related to: (i) higher rutile content (Table 2), (ii) larger grains (Fig. 6); an important role of crystallite and particle size in nanocrystalline TiO₃-based photocatalysts is realized mostly through influencing the dynamics of e-/h+ recombination and adsorption at the surface [41,42], (iii) other surface properties such as acidity, hydrophobicity and magnetic-surface interactions, which have not been studied in detail. Accounting for the differences in the preparation modes of the two catalysts the later variations are rather possible.

A positive effect of the NT addition to the sol-gel product is significant in the first stage of the process up to 45 min illumination and can be related to the larger BET surface and micropore area of the NT-containing product (Table 3) leading to higher sorption (Table 5). However, after that, the plateau in the relation $-\ln(C/C_0)/t$ is observed to have a very low rate constant (Fig. 12, Table 5). If one considers the rate constant average value (Table 5), the overall effect of NT presence is rather low

²Second stage of the process

Table	6.	Effectiveness of some methods for photocatalytic degradation of EE2.
--------------	----	--

Reference	Estrogen initial concentration, μΜ	Illumination	Rate constant, k×10 ⁻³ min ⁻¹	Degradation (%) - for time (min)
[7] [9]	3	125 W, UVA, UVB, UVC UVA	231	25 - 180
[8] This work	0.033 1.0	UVA 17 W, UVA	86 315 (P25)	100 – 15

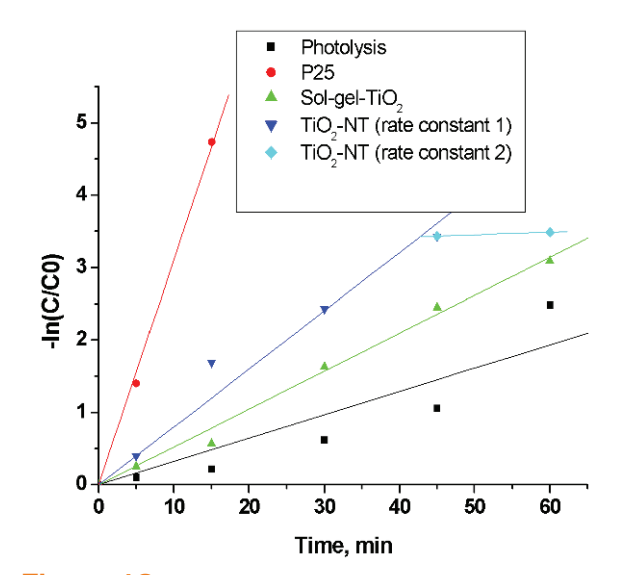


Figure 12. Pollutant degradation as a function of irradiation time in presence of different catalysts.

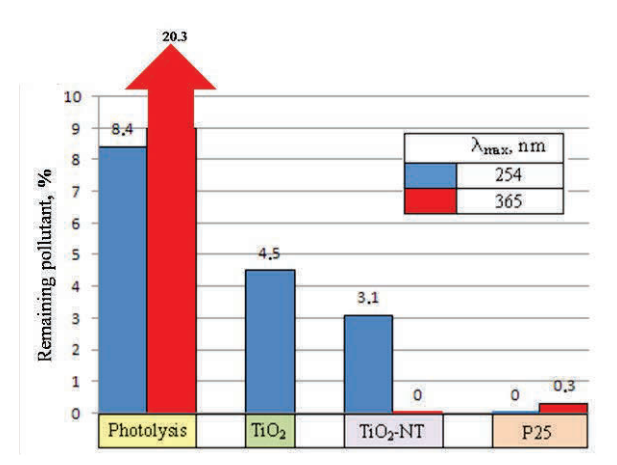


Figure 13. Remaining pollutant (%) after 60 min illumination with UV-light with λ_{max}=254 nm or λ_{max}=365 nm in presence of different catalysts.

– the reaction rate constant increases with only ~10% (the same result is reported in [17] for a composite with a similar composition as the one used in the present paper) and the ratio $[R(P25)/R_1(TiO_2-NT)]_{254}$ nm = 3.9 (R – rate constant, R_1 –first stage rate constant).

The comparison of the results (Table 5, Fig.13) from the photocatalytic tests under different wavelength UV irradiation is complicated due to great differences in illumination source power. As can be expected, the effect of photolysis decreases significantly with the increase of the illumination light wavelength. This factor dominates over the lamp power. The photocatalytic performance of TiO₂-NT follows the opposite trend – the rate constant at longer wavelength irradiation is almost doubled compared with its average value observed at illumination with λ_{max} = 254 nm demonstrating the role of the light intensity. The case with TiO2-P25 is more specific. At UVC irradiation applied in the present work, a one stage first order process is clearly expressed leading to full destruction of the EE2 after 15 min irradiation. Data in [15] show that at UVA illumination a 15 min-initial period with a very high photocatalytic activity is followed by a stage of much slower degradation of the pollutant. Even if we choose to consider the value of the first stage rate constant, the ratio $[R_1(P25)/R(TiO_2-NT)]_{365 \text{ nm}} = 3.4 \text{ is}$ obtained, i.e., the advantage of TiO2-P25 over TiO2-NT decreases with the irradiation wave-length increase. Furthermore, at these illumination conditions, P25 does not ensure complete destruction of the pollutant within 60 min illumination (Fig. 13). Overall, the results suggest that the influence of the illumination light wavelength, intensity and catalyst nature are linked.

Table 6 compares the obtained results on the photocatalytic degradation rate constants and the pollutant destruction degree to some literature data. It is seen that complete destruction of the pollutant can be reached for 15 min at short length irradiation on Degussa P25.

4. Conclusions

The paper gives a detailed description of the crystal structure, textural properties, sorption and performance for photocatalytic destruction of EE2 by the commercial product Degussa P25, sol-gel prepared ${\rm TiO_2}$ calcined at different temperatures and ${\rm TiO_2}$ doped with carbon nanotubes. It has been established that:

- The commercial product TiO_2 P25 showed significant degradation efficiency for EE2 under UV (λ_{max} =254 nm) light. The pure TiO_2 sol-gel synthesized at 700°C is ~6-fold less effective than Degussa P25.

Higher rutile content, larger grains and other surface properties (acidity, hydrophobicity, etc.) seem to be among the factors responsible for the low efficiency of the sol-gel product.

- The addition of carbon nanotubes to the similar (lower temperature produced) ${\rm TiO_2}$ leads to an increase of the catalyst activity in the first stage of the photocatalytic process but its overall effect after 1 h irradiation is insignificant at the applied photocatalytic test conditions.
- The product TiO₂ Degussa P25 is an appropriate catalyst for EE2 degradation when UVA irradiation is applied, ensuring its full destruction in 30 min.

References

- [1] T. Heberer, Toxicol. Lett. 131, 5 (2002)
- [2] P. Adler, Th. Steger-Hartmann, W. Kalbfus, Acta Hydrochim. Hydrobiol. 29, 227 (2001) (in German)
- [3] C.E. Purdom, P.A. Hardiman, V.J. Bye, N.C. Eno, C.R. Tyler, J.P. Sumpter, Chem. Ecol. 8, 275 (1994)
- [4] A.C. Johnson, J.P. Sumpter, Environ. Sci. Technol. 35, 4697 (2001)
- [5] C. Desbrow, E.J. Routledge, G.C. Brighty, J.P. Sumpter, M. Waldock, Environ. Sci. Technol. 32, 1549 (1998)
- [6] H.M. Coleman, B.R. Eggins, J.A. Byrne, F.L. Palmer, E. King, Appl. Catal. B 24, L1 (2000)
- [7] H.M. Coleman, M.I. Abdullah, B.R. Eggins, F.L. Palmer, Appl. Catal. B 55, 23 (2005)
- [8] H.M. Coleman, E.J. Routledge, J.P. Sumpter, B.R. Eggins, J.A. Byrne, Water Res. 38, 3233 (2004)
- [9] G. Li Puma, V. Puddu, H.K. Tsang, A. Gora, B. Toepfer, Appl. Catal. B 99, 388 (2010)
- [10] T. Nakashima, Y. Ohko, D.A. Tryk, A. Fujishima, J. Photochem. Photobiol. A 151, 207 (2002)
- [11] Y. Ohko, K. Iuchi, Ch. Niwa, T. Tatsuma, T. Nakashima, T. Iguchi, Y. Kubota, and A. Fujishima, Environ. Sci. Technol. 36, 4175 (2002)
- [12] H.M. Coleman, K. Chiang, R. Amal, Chem. Eng. J. 113, 65 (2005)
- [13] Y. Zhang, J.L. Zhou, B. Ning, Water Res. 41, 19 (2007)
- [14] T. Nakashima, Y. Ohko, Y. Kubota, A. Fujishima, J. Photochem. Photobiol. A 160, 115 (2003)
- [15] W. Wang, Ph. Serp, Ph. Kalck, Cl.G. Silva, J. L. Faria, Mater. Res. Bull. 43, 958 (2008)
- [16] Y. Yu, J.C. Yu, J.-G. Yu, Y.-Ch. Kwok, Y.-K. Che, J.-C. Zhao, L. Ding, W.-K. Ge, P.-K. Wong, Appl. Catal. A 289, 186 (2005)
- [17] W. Wang, P. Serp, P. Kalck, J.L. Faria, J. Mol. Catal. A: Chem. 235, 194 (2005)

Acknowledgments

The work was performed with the financial support of the Slovenian Research Agency (research program P2-0150) and the Bulgarian Fund for Scientific Investigations (Contract DO 02-93/08).

- [18] J. Birkenstock, R.X. Fischer, T. Messner, BRASS 1.0 beta: The Bremen Rietveld Analysis and Structure Suite. Zentrallabor für Kristallographie und Angewandte Materialwissenschaften, Fachbereich Geowissenschaften (University of Bremen, Bremen, 2003)
- [19] B. Lei, Sh. Huang, Y. Zhou, D. Wang, Z. Wang, China, Chemosphere 76, 36 (2009)
- [20] R. Jeannot, H. Sabik, E. Sauvard, T. Dagnac, K. Dohrendorf, J. Chromatogr. A 974, 143 (2002)
- [21] R.A. Trenholm, B.J. Vanderford, J.C. Holady, D.J. Rexing, S.A. Snyder, Chemosphere 65, 1990 (2006)
- [22] A.-W. Xu, Y. Gao, H.-Q. Liu, J. Catal. 207, 151-157 (2002)
- [23] C. Huang, W. You, L. Dang, Z. Lei, Z. Sun, L. Zhang, Chin. J. Catal. 27, 203 (2006)
- [24] Y. Zhang, H. Xu, Y. Xu, H. Zhang, Y. Wang, J. Photochem. Photobiol. A 170, 279 (2005)
- [25] J. Yu, H. Yu, B. Cheng, M. Zhou, X. Zhao, J. Mol. Catal. A: Chem. 253, 112 (2006)
- [26] M. Kruk, M. Jaroniec, Chem. Mater. 13, 3169 (2001)
- [27] K.S.W. Sing, D.H. Everett, R.A.W. Haul, L. Moscou, R.A. Pierotti, J. Rouquerol, T. Siemieniewska, Pure Appl. Chem. 57, 603 (1985)
- [28] J.-h. Xu, W.-L. Dai, J. Li, Y. Cao, H. Li, H. He, K. Fan, Catal. Commun. 9, 146 (2008)
- [29] Y. Zhang, H. Zhang, Y. Xu, Y. Wang, J. Solid State Chem. 177, 3490 (2004)
- [30] T. Ohsaka, F. Izumi, Y. Fujiki, J. Raman Spectrosc. 7, 321 (1978)
- [31] H.X. Li, J.X. Li, Y.I. Huo, J. Phys. Chem. B 110, 1559 (2006)
- [32] J. Geng, D. Yang, J. Zhu, D. Chen, Z. Jiang, Mater. Res. Bull. 44, 146 (2009)
- [33] Z. Zhang, Ch.-Ch. Wang, R. Zakaria, J.Y. Ying, J. Phys. Chem. B 102, 10871 (1998)

- [34] T. Ohno, K. Sarukawa, K. Tokieda, M. Matsumura, J. Catal. 203, 82 (2001)
- [35] R.I. Bickley, T. Gonzalez-Carreno, J.S. Lees, L. Palmisano, R.D.J. Tilley, J. Solid State Chem. 92, 178 (1991)
- [36] W. Wang, P. Serp, P. Kalck, C.G. Silva, J.L. Faria, Mater. Res. Bull. 43, 958 (2008)
- [37] D.S. Todorovsky, R.V. Todorovska, St. Groudeva-Zotova, Mat Lett 55, 41 (2002)
- [38] Z. Lin, A. Orlov, R.M. Lambert, M.C. Payne, J. Phys. Chem. B 109, 20948 (2005)

- [39] B. Pan, D. Lin, H. Mashayekhi, B. Xing, Environ. Sci. Technol. 42, 5480 (2008)
- [40] K. Bubacz, J. Choina, D. Dolat, E. Borowiak-Paleń, D. Moszyński, A.W. Morawski, Mater. Res. Bull. 45, 1085 (2010)
- [41] R. Scotti, M. D'Arienzo, F. Morazzoni, I. R. Bellobono, Appl. Catal. B 88, 323 (2009)
- [42] A. Testino, I.R. Bellobono, V. Buscaglia, C. Canevali, M. D'Arienzo, S. Polizzi, R. Scotti, F. Morazzoni, J. Am. Chem. Soc. 129, 3564 (2007)